Self-Assembled Triangular and Labyrinth Buckling Patterns of Thin Films on Spherical Substrates

Guoxin Cao and Xi Chen*

Department of Civil Engineering and Engineering Mechanics, Columbia University, New York, New York 10027-6699, USA

Chaorong Li

Optoelectronics Materials and Devices, Department of Physics and Key Laboratory of Advanced Textile Materials and Manufacturing Technology Ministry of Education, Zhejiang Sci-Tech University, Hangzhou 310018, China

Ailing Ji and Zexian Cao

Institute of Physics, Chinese Academy of Sciences, P.O. Box 603, 100080 Beijing, China

(Received 28 September 2007; published 23 January 2008)

We investigated the possibility of controlling thin film buckling patterns by varying the substrate curvature and the stress induced therein upon cooling. The numerical and experimental studies are based on a spherical Ag core/SiO_2 shell system. For Ag substrates with a relatively larger curvature, the dentlike triangular buckling pattern comes out when the film nominal stress exceeds a critical value. With increasing film stress and/or substrate radius, the labyrinthlike buckling pattern takes over. Both the buckling wavelength and the critical stress increase with the substrate radius.

DOI: 10.1103/PhysRevLett.100.036102 PACS numbers: 68.55.−a, 65.40.De, 68.18.Fg, 68.35.Gy

Spontaneous formation of ordered buckling patterns in thin films deposited on compliant substrates has attracted recent attention, which may hold promise for fabrication based on self-assembly [1,2], stretchable large-area interconnects [3], and measuring film elastic properties [4], among others. Bowden *et al.* [5] found that when a metal thin film is deposited on a thick elastomer substrate, the large mismatch between the coefficients of thermal expansion (CTE) of the metal and elastomer produces an equibiaxial compression in film when the system is cooled; the film begins to buckle elastically at a critical temperature, and, upon further cooling, the buckle amplitude grows (but the buckle wavelength is unaltered) while the film remains bonded to the substrate. Similar phenomena can be observed when a thin film is created via oxidation [6] or modification [7] of the surface properties of the substrate. Interestingly, whenever the substrate is sufficiently flat, the zigzag labyrinthlike buckling pattern [8] (or herringbone pattern [9,10]) is the most favorable occurrence when the film is under equibiaxial compression.

Extensive studies, both experimental and theoretical, have been employed to investigate the mechanism and feasibility of manipulating buckled films on compliant substrates so as to achieve highly ordered patterns. By selectively patterning the substrate (changing the modulus [7] or the topology of the substrate surface [5], or depositing the film within a small patterned substrate surface area [11]), the buckles are confined into small regions with distinct features, which are due to the stress perturbation induced by the confining substrate features.

Theoretically, it was shown that among various competitive modes, the herringbone mode possesses the lowest strain energy for a planar film under equibiaxial compression [9], and, thus, justifies its existence in various natural circumstances [5]. The feature of the labyrinthlike buckling pattern also depends on the anisotropy of the film stress [12–14], which suggests that by constraining the film-substrate system to create nonequibiaxial stresses, the buckling patterns may be controlled [10]. Over this topic general wrinkling theory was presented [15,16].

However, most previous studies focused on the buckling arising in the planar geometry, and the effect of the curvature of the substrate was untouched. It is well known that the buckling of thin shells is highly sensitive to the shell curvature [17,18], but to the best of our knowledge, the mechanism of spontaneous buckling pattern formation in thin films on curved substrates (without delamination) has not yet been studied. In addition, the buckling behavior on a closed surface will differ from that on a surface with free boundaries, since they are topologically distinct geometrical objects: the closed 2D surface such as a sphere has genus 0, whereas for a surface of free boundaries, planar or curved, it has genus 1. Therefore, the buckling patterns on a sphere will manifest some features primarily arising from the topological constraint. Li *et al.* [19–21] reported that the triangular patterns can self-assemble on the surface of a SiO_2 shell on spherical Ag core structure by cooling; however, the key issues regarding the effect of substrate curvature on buckling patterns, and the evolution of pattern with increased film stress, are not explored—it is expected that the investigation of such a problem may be helpful to the understanding of pattern formation on receptacles of plants, on clusters of colloidals, and on the crystallizing liquid (metal and helium) drops, etc., where the strategy for a minimum energy configuration has to be conformed with the geometry of the support [19–21].

Consider a compliant spherical substrate with radius R, Young's modulus E_s, and Poisson's ratio ν_s; a stiffer film with a uniform thickness h, characterized by a Young's modulus E and a Poisson's ratio ν, is deposited onto the substrate and remains bonded at all times. The CTEs of film and substrate are α and α_s, respectively, with $\alpha_s > \alpha$. Here, R and h are geometrical features and the other parameters are material properties. As the temperature is lowered by a magnitude of ΔT, the substrate contraction imposes a radial pressure on the interface. From the continuity of pressure and circumferential strain at the interface, the magnitude of the compressive hoop stress in the film can be derived analytically:

$$\sigma_f = \frac{EE_s(3R^3 + 3R^2h + 3Rh^2 + h^3)(\alpha_s - \alpha)\Delta T}{3E_sR^3(1-\nu) + E_s(1+\nu)(3R^2h + 3Rh^2 + h^3) + 2E(1-2\nu_s)h(3R^2 + 3Rh + h^2)}. \quad (1)$$

When $R/h \to \infty$ it reduces to the well-known relationship for planar film on a semi-infinite substrate [9]:

$$\sigma_f(R/h \to \infty) \equiv \sigma_\infty = E(\alpha_s - \alpha)\Delta T/(1-\nu). \quad (2)$$

For a model system with the following typical properties: $E = 75$ GPa, $\nu = 0.17$, $\alpha = 0.45 \times 10^{-6}$/K, $E_s = 25$ GPa, $\nu_s = 0.37$, $\alpha_s = 115 \times 10^{-6}$/K, and $h = 150$ nm, which corresponds to the Ag core/SiO_2 shell in parallel experiments. σ_f/σ_∞ increases nonlinearly with R/h, and when R/h exceeds about 50, σ_f/σ_∞ approaches 1 and becomes relatively insensitive to the substrate curvature.

Numerical simulations are carried out using the finite element method (FEM) [22]. The buckling behavior varying with R and ΔT was investigated based on the geometrical and material parameters given above. To be consistent with the analytical solution, we assume an ideal thermal conduction with uniform temperature in the system. All material properties are assumed as invariants in the temperature range concerned [23]. The prebuckling stress computed from FEM agrees well with (1), which validates the numerical approach.

From dimensional analysis, the normalized substrate radius of curvature, R/h, is the only governing geometrical parameter of the system under investigation. We have confirmed from FEM analyses that while h may also be variable, as long as R/h is fixed, all results presented in this Letter are the same. For a given R/h, the nominal stress σ_f in the film, following Eq. (1), will be continuously reinforced with increasing ΔT until the film starts to buckle at a critical stress σ_C; consequently, the hoop stress is partially relieved. Afterwards, with further increasing of ΔT, the buckle amplitude grows and the buckling pattern evolves to minimize the total strain energy. When the material parameters are fixed, a map of buckling patterns can be plotted varying with regard to the normalized substrate curvature and the nominal film stress. In Fig. 1, the white (light) color shows the concave "bottom" of buckles, and the particle radii are rescaled to fit into the map (in the two-color contour plot, the dark means that in this region the radial displacement magnitude is smaller than a certain value). Note that in order to initiate buckling, a very small random perturbation is introduced to the system. Although such a numerical "defect" affects the initial buckling formation just above the critical stress, it has no influence on the value of σ_C as well as the final appearance of buckling patterns, which are governed by strain energy of the entire system and insensitive to the initial perturbation [9].

When the substrate curvature is relatively large, just above σ_C the dentlike buckles appear, which soon assemble into a triangular pattern at $\sigma_f/\sigma_C > 1.05$. Since the dents are concave structures generated from the initially convex surface, it involves both bending and stretching energies, with the latter component more dominant [9]. With the continued cooling the buckle amplitude increases and several neighboring dents may merge to elliptical dents so as to alleviate the stretching energy, yet roughly speaking, the dentlike buckles persist since they are constrained by the large curvature of substrate. In the case of $R/h =$ 20–40, the triangular dentlike buckle pattern first forms when σ_f is just above σ_C, but with further cooling it evolves into a labyrinthlike pattern, as a consequence of extensive coalescence of small dents; the details of the labyrinth also vary with σ_f/σ_C so as to minimize the strain energy.

For larger particles, the labyrinthlike buckle forms immediately when the film is overstressed and persists with

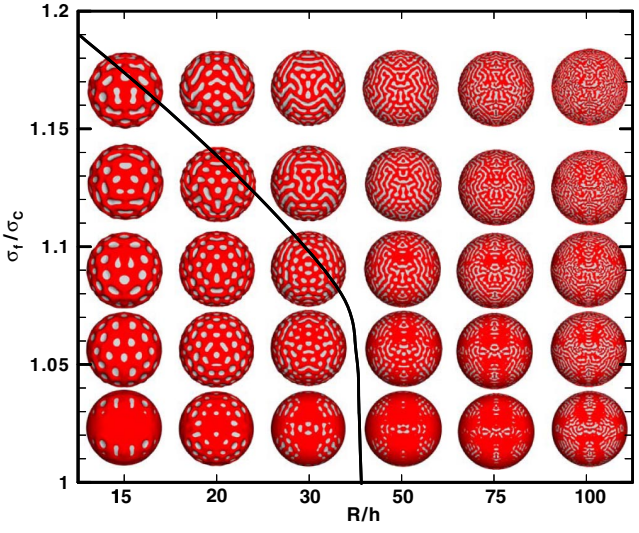

FIG. 1 (color online). The map of buckling patterns for Ag core/SiO_2 shell systems plotted against the normalized film nominal stress (vertical axis) and the normalized substrate radius of curvature R/h (horizontal axis).

the increasing film stress. Note that labyrinth patterns are expected for planar films (with $R/h \rightarrow \infty$) [9,12–14]. Therefore, when both σ_f/σ_C and R/h are small, the triangularly distributed dentlike pattern is expected; otherwise, the labyrinthlike pattern dominates, and a clear transition boundary between these two categories is identifiable for the current model system, as sketched in Fig. 1.

The two most important features that characterize the buckling behavior are the buckle wavelength and critical stress. The wavelength, L_C, is measured as the averaged spacing between the bottom (lowest point) of neighbor buckles. For a given R/h, although the buckling pattern may evolve with σ_f/σ_C, the wavelength is unchanged. The variation of L_C/R is plotted as a function of R/h in Fig. 2, where the magnitude of L_C increases with the particle radius. A power-law relationship can be fitted, $L_C/R = a(R/h)^b$, with $a = 3.0$ and $b = -0.8$ for the current range of particle size and material parameters. In the limit of $R/h \rightarrow \infty$, the buckling wavelength of a planar thin film on semi-infinite substrate is [9]

$$L_C(R/h \rightarrow \infty) = 2\pi h[E/E_s(1 - \nu_s^2)/(1 - \nu^2)]^{1/3}, \quad (3)$$

which agrees reasonably well with the results in Fig. 2. It follows that L_C is moderately affected by the substrate curvature, especially when the curvature is large, whereas for larger particles L_C becomes relatively less insensitive to R/h.

For $R/h \rightarrow \infty$, the critical buckling stress is [9]

$$\sigma_C^0 = [E/(1 - \nu^2)]^{1/3}[3E_s/(1 - \nu_s{}^2)]^{2/3}/4. \quad (4)$$

As R/h is varied, the normalized critical buckling stress, σ_C/σ_C^0, is plotted in Fig. 2. The σ_C/σ_C^0 varies almost linearly within the current range of R/h; in the limit of $R/h \rightarrow \infty$, σ_C/σ_C^0 should converge to unity. Evidently, the substrate curvature has a significant impact on the critical buckling stress.

To validate the simulation result that the spontaneous buckling pattern depends strongly on the radius of substrate, Ag core/SiO_2 shell microstructures were prepared at high temperature via thermal evaporation in the parallel experiment. A mixture of high-purity SiO and Ag_2O powders was used as the precursor, and the evaporation was done in an Al_2O_3 crucible enclosed in a reaction chamber. The chamber was first evacuated to less than 10 Pa, and then filled with a gas mixture of 90%Ar + 10% H2 to a pressure of 3×10^4 Pa. A sapphire substrate was held at within 1 cm over the precursor surface to collect the evaporation products. As the first step, the crucible containing the powder mixture was heated to ~1535 K, and the substrate was held at ~1270 K, a temperature just above the melting point of silver (1234.8 K) but far below that of SiO_2 (1883 K) in order to favor the formation of Ag core/SiO_2 shell microstructures. Liquid droplets with a radius of about 1–50 microns formed on the way flying to the substrate. Because of the low solubility of SiO_2 in Ag, a Ag core/SiO_2 shell structure results through interdiffusion, which is composed of a SiO_2 layer with a thickness of about 150 nm (measured from some broken shells with SEM) covering uniformly on the soft Ag core. The final thickness of the SiO_2 layer was controlled by changing composition of the precursor mixture. After maintaining the system at given temperatures for about 15 minutes, the system was let cool down at a moderate cooling rate of about 4–5 K/ sec (a very fast cooling rate may rupture the structure or crack the shell). Those core/shell structures just arriving at the substrate now may or may not get wrinkled and are available for later observation. *Ex situ* observation of the patterns was performed on a scanning electron microscope (SEM; FEI, SERION) operated at 5.0 KeV. The long depth of field of electron microscope enables the clear imaging of the structure details on a curved surface; hence, all the patterns on the core/shell structures can be imaged. Chemical compositions of Ag,

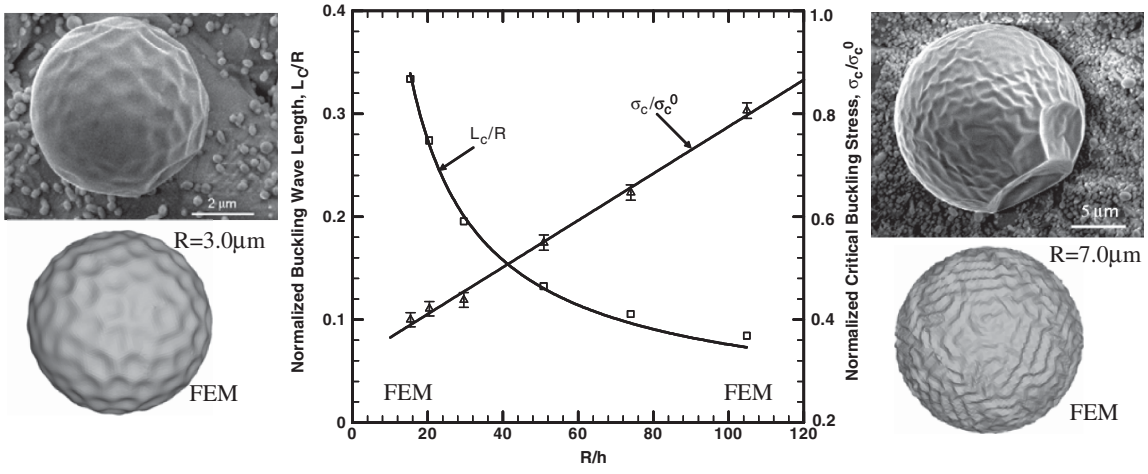

FIG. 2. FEM results of variation of the normalized critical buckling wavelength, L_C/R, and the critical buckling stress, σ_C/σ_C^0, as a function of R/h. Also shown are comparison between the simulated buckling patterns and SEM micrographs on Ag core/SiO_2 shell system, with $R = 3.0$ μm and 7.0 μm.

Si, and O are conformed by the energy-dispersive x-ray spectrometer attached to the SEM.

Figure 2 shows SEM photos and FEM simulations of the typical buckle patterns observed in small and large particles, respectively: there is a good agreement in the buckled shape as well as in the buckling wavelength. It is validated that the triangular dentlike pattern is preferred when the substrate curvature is large, whereas the labyrinthlike pattern dominates in larger particles.

Although some surface instabilities are known to be another factor of causing wrinkling at the surface of a stressed solid [24–27], we note that the amplitudes of patterns observed in experiment (Fig. 2) are typical for buckles. Moreover, based on a first-order estimation [28], the wavelengths of the most unstable mode for a planar substrate are $4\pi E\gamma/(3\sigma^2)$ and $2\pi E\gamma/\sigma^2$, respectively, for the surface diffusion and evaporation-condensation driven surface instability. For SiO_2, the surface energy $\gamma = 1.5\ \mathrm{J/m^2}$, and, if we take the stress $\sigma = \sigma_f \approx \sigma_\infty$ [Eq. (1)], the instability wavelengths are estimated to be about 4.7 and 7.0 nm, respectively. Both values are much smaller than that observed in Fig. 2 where the wavelength is on the order of microns, thus confirming that surface instability can be neglected in this study.

To summarize, both numerical and experimental analyses were carried out to investigate the effect of substrate curvature and film stress on thin film buckling patterns. The study is based on a SiO_2 film/Ag spherical substrate assembly, yet the main findings are applicable to other similar stiff film/compliant substrate systems. The transition of buckling patterns has been observed when either the curvature of the system or the stress developed by cooling is changed. The triangular dentlike buckles are preferred in smaller particles (due to the strong effect of curvature), whereas the labyrinthlike pattern dominates the larger particles. With the increased film stress in small or intermediate particles, the dents coalescence to reduce the stretching energy and gradually evolve into labyrinthlike patterns. When the substrate radius is less than about 50 times the film thickness, the substrate curvature strongly influences the nominal film stress as well as the critical buckling wavelength. The critical buckling stress is very sensitive to the underlying substrate curvature and can be significantly reduced by enlarging the curvature of the core/shell structure. When the core size gets very big, all numerical solutions converge to that for a planar film bound on a semi-infinite substrate. The parallel experiments have verified the dominance of the triangularly distributed dentlike patterns in smaller particles and the formation of the labyrinthlike patterns in larger particles. These results serve as a first attempt of controlling thin film buckling patterns via the variation of substrate curvature, which may promise potential applications in a variety of areas.

The numerical study of this research was supported by NSF No. CMMI-0643726, while the experimental work was financed by the NSFC, the Science Foundation of ZSTU, and the Civil Space Exploration Program of China.

*Corresponding author.
xichen@civil.columbia.edu

[1] P. J. Yoo, K. Y. Suh, S. Y. Park, and H. H. Lee, Adv. Mater. **14**, 1383 (2002).
[2] P. J. Yoo and H. H. Lee, Phys. Rev. Lett. **91**, 154502 (2003).
[3] S. Lacour, S. Wagner, Z. Huang, and Z. Suo, Appl. Phys. Lett. **82**, 2404 (2003).
[4] C. M. Stafford, C. Harrison, K. L. Beers, A. Karim, E. J. Amis, M. R. Vanlandingham, H. C. Kim, W. Volksen, R. D. Miller, and E. E. Simonyi, Nat. Mater. **3**, 545 (2004).
[5] N. Bowden, S. Brittain, A. G. Evans, J. W. Hutchinson, and G. M. Whitesides, Nature (London) **393**, 146 (1998).
[6] N. Bowden, W. T. S. Huck, K. E. Paul, and G. M. Whitesides, Appl. Phys. Lett. **75**, 2557 (1999).
[7] W. T. S. Huck, N. Bowden, P. Onck, T. Pardoen, J. W. Hutchinson, and G. M. Whitesides, Langmuir **16**, 3497 (2000).
[8] L. Mahadevan and S. Rica, Science **307**, 1740 (2005).
[9] X. Chen and J. W. Hutchinson, J. Appl. Mech. **71**, 597 (2004).
[10] X. Chen and J. W. Hutchinson, Scr. Mater. **50**, 797 (2004).
[11] E. P. Chan and A. J. Crosby, Adv. Mater. **18**, 3238 (2006).
[12] Z. Huang, W. Hong, and Z. Suo, Phys. Rev. E **70**, 030601 (2004).
[13] R. Huang, J. Mech. Phys. Solids **53**, 63 (2005).
[14] Z. Y. Huang, W. Hong, and Z. Suo, J. Mech. Phys. Solids **53**, 2101 (2005).
[15] E. Cerda and L. Mahadevan, Phys. Rev. Lett. **90**, 074302 (2003).
[16] J. Genzer and J. Groenewold, Soft Matter **2**, 310 (2006).
[17] A. Libai and J. G. Simmons, *The Nonlinear Theory of Elastic Shells* (Cambridge University Press, Cambridge, 1998).
[18] J. W. Hutchinson, J. Mech. Phys. Solids **49**, 1847 (2001).
[19] C. Li, X. Zhang, and Z. Cao, Science **309**, 909 (2005).
[20] X. N. Zhang, C. R. Li, Z. Zhang, and Z. X. Cao, Appl. Phys. Lett. **85**, 3570 (2004).
[21] C. Li, A. Ji, and Z. Cao, Appl. Phys. Lett. **90**, 164102 (2007).
[22] ABAQUS, *ABAQUS 6.4 User's Manual* (ABAQUS Inc., Pawtucket, Rhode Island, 2004).
[23] F. Kakinuma and Y. Tsuchiya, J. Phys. Soc. Jpn. **70**, 2948 (2001).
[24] R. J. Asaro and W. A. Tiller, Metall. Mater. Trans. B **3**, 1789 (1972).
[25] J. Colin, Int. J. Solids Struct. **44**, 3218 (2007).
[26] J. Muller and M. Grant, Phys. Rev. Lett. **82**, 1736 (1999).
[27] M. Grinfeld, Europhys. Lett. **22**, 723 (1993).
[28] D. J. Srolovitz, Acta Metall. **37**, 621 (1989).